Monthly Notices
of the
ROYAL ASTRONOMICAL SOCIETY

MNRAS **429,** 903–914 (2013) doi:10.1093/mnras/sts386

New brown dwarf discs in Upper Scorpius observed with *WISE*

P. Dawson,[1⋆] A. Scholz,[1] T. P. Ray,[1] K. A. Marsh,[2] K. Wood,[3] A. Natta,[1,4] D. Padgett[5] and M. E. Ressler[6]

[1]*School of Cosmic Physics, Dublin Institute for Advanced Studies, 31 Fitzwilliam Place, Dublin 2, Ireland*
[2]*School of Physics and Astronomy, Cardiff University, Cardiff CF24 3AA*
[3]*School of Physics and Astronomy, University of St Andrews, North Haugh, St Andrews KY16 9SS*
[4]*INAF – Osservatorio Astrofisico di Arcetri, Largo E. Fermi 5, I-50125 Firenze, Italy*
[5]*Goddard Space Flight Center, Greenbelt, MD 20771, USA*
[6]*Jet Propulsion Laboratory, California Institute of Technology, 4800 Oak Grove Drive, Pasadena, CA 91109, USA*

Accepted 2012 November 8. Received 2012 October 12

ABSTRACT

We present a census of the disc population for UKIDSS selected brown dwarfs in the 5–10 Myr old Upper Scorpius OB association. For 116 objects originally identified in UKIDSS, the majority of them not studied in previous publications, we obtain photometry from the *Wide-Field Infrared Survey Explorer* data base. The resulting colour–magnitude and colour–colour plots clearly show two separate populations of objects, interpreted as brown dwarfs with discs (class II) and without discs (class III). We identify 27 class II brown dwarfs, 14 of them not previously known. This disc fraction (27 out of 116, or 23%) among brown dwarfs was found to be similar to results for K/M stars in Upper Scorpius, suggesting that the lifetimes of discs are independent of the mass of the central object for low-mass stars and brown dwarfs. 5 out of 27 discs (19 per cent) lack excess at 3.4 and 4.6 μm and are potential transition discs (i.e. are in transition from class II to class III). The transition disc fraction is comparable to low-mass stars. We estimate that the time-scale for a typical transition from class II to class III is less than 0.4 Myr for brown dwarfs. These results suggest that the evolution of brown dwarf discs mirrors the behaviour of discs around low-mass stars, with disc lifetimes of the order of 5–10 Myr and a disc clearing time-scale significantly shorter than 1 Myr.

Key words: techniques: photometric – open clusters and associations: individual: Upper Scorpius – infrared: stars.

1 INTRODUCTION

Brown dwarfs – substellar objects with masses below the Hydrogen burning limit of 0.08 $M_{\odot}$ – are ideal to test the mass dependence of critical parameters in stellar evolution. One example for such a parameter is the lifetime of circumstellar discs, which is an important constraint for the core-accretion scenarios for planet formation. The disc lifetime is affected by a number of physical processes, e.g. disc ionization by the central object and cosmic rays, accretion, grain growth (e.g. Dullemond et al. 2007). Our understanding of the relative importance of these processes and how they change with object mass is still incomplete, i.e. observational guidance is important to advance the theory.

The clear majority of low-mass stars lose their disc within less than 5 Myr (Haisch, Lada & Lada 2001; Jayawardhana et al. 2006). Maybe the best test for the longevity of discs is the Upper Scorpius OB association (UpSco in the following), the oldest nearby star-forming region with a substantial number of brown dwarfs. UpSco is often assumed to have an age of 5 Myr (Preibisch et al. 2002) but recently Pecaut, Mamajek & Bubar (2012) have derived an older age of 10 Myr for this region. In UpSco, Carpenter et al. (2006) derived a disc frequency of <8 per cent for F and G stars and 19 ± 4 per cent for K0–M5 stars (with 1σ binomial confidence intervals). The brown dwarfs in this region exhibit a disc fraction of 37 ± 9 per cent, based on an examination of 35 objects (Scholz et al. 2007). Thus, the *Spitzer* data tentatively show that the disc fractions *in UpSco increase monotonically with decreasing object mass for early F- to late M-type objects*. This would imply a mass dependence in the disc evolution, resulting in long-lived discs in the substellar regime.

So far, the brown dwarf disc frequency in UpSco is affected by low number statistics. Here we set out to test previous findings based on a much enlarged number of brown dwarfs in UpSco, identified from UKIDSS. To identify the objects in our sample that have a disc (class II objects) and those that do not (class III objects), we use

⋆ E-mail: dawsonp@tcd.ie

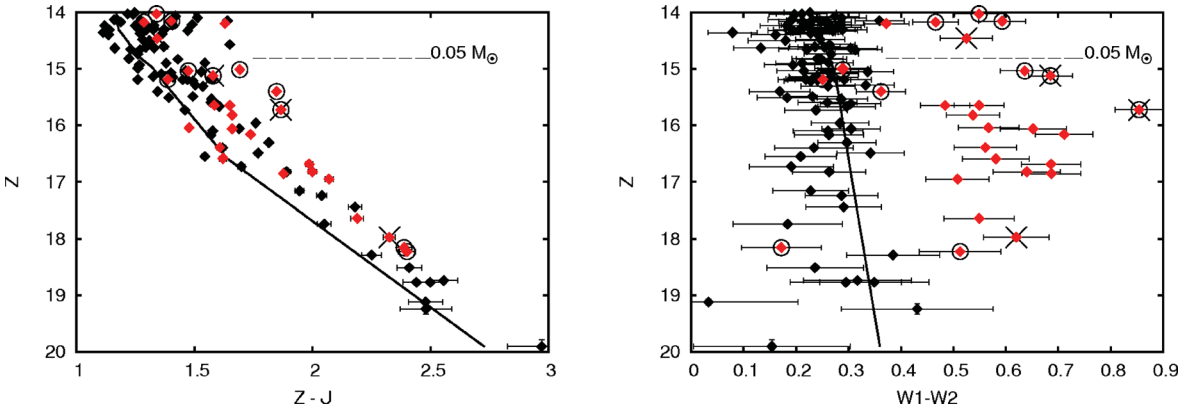

Figure 1. ($Z-J$,Z) and ($W1-W2$,Z) colour–magnitude diagrams for 116 out of 119 brown dwarfs identified in UpSco for which *WISE* data were available. The class II objects are marked in red in the online version of this paper. The 5 Myr DUSTY model (Chabrier et al. 2000) isochrones are also shown with mass decreasing from 0.09 (top) to 0.01 $M_{\odot}$ (bottom). The 0.05 $M_{\odot}$ positions on the isochrones are indicated. In the ($Z-J$, Z) diagram all the objects are grouped close to the isochrone and none show any significant colour excess. However, two distinct populations of objects are clearly visible in the ($W1-W2$,Z) diagram, one close to the isochrone and one showing an excess in $W1-W2$. The 11 objects ringed have bright unambiguous signals in $W4$ (22 μm), diagnostic of the presence of a disc (see the text; Section 4.1.4). The four objects marked with a cross have significant variations in their UKIRT and 2MASS J or H magnitudes, a characteristic associated with accretion events or variable extinction (also see the text; Section 4.2).

data from the *Wide-Field Infrared Survey Explorer* (*WISE*) (Wright et al. 2010). As will be shown, with improved statistics we find a disc fraction for brown dwarfs that is consistent with the value published for low-mass stars in this region.

2 TARGETS

Dawson, Scholz & Ray (2011) identified 19 new brown dwarf candidates in the south of UpSco via a photometric and proper motion analysis of UKIDSS data. The level of contamination from background stars in the sample was shown to be negligible. Using the same method in the north of UpSco a further 49 objects previously identified by Lodieu, Hambly & Jameson (2006) and Lodieu et al. (2007) as brown dwarf candidates were recovered. Spectra have been taken of 26 of these 49 objects (Martin, Delfosse & Guieu 2004; Lodieu et al. 2006, 2008; Slesnick, Carpenter & Hillenbrand 2006; Lodieu, Dobbie & Hambly 2011) and all 26 have been confirmed as brown dwarfs. This provides a sample of 68 very low-mass stellar and substellar objects in UpSco. Dawson et al. (2011) determined that the 68 objects ranged in mass from 0.01 to 0.09 $M_{\odot}$ by comparing their observed Z magnitudes with theoretical Z magnitudes from the DUSTY models for 5 Myr old objects.

Dawson et al. (2011) used the Eighth Data Release from UKIDSS to identify the new brown dwarfs. Since then, UKIDSS has issued a Ninth Data Release which covers a substantially larger area in UpSco. Using the same method as in Dawson et al. (2011), we have identified a further 51 objects in the same mass range to add to the sample. The details of this extended survey are given in Appendix A. The addition of these new objects increases the size of the homogeneous sample of objects uniformly selected via their colour and proper motion characteristics to 119. Although some objects in our sample may be slightly above the substellar threshold, we will refer to our targets as 'brown dwarfs' throughout this paper, for simplicity.

All 119 objects lie close to the 5 Myr DUSTY model isochrones of Chabrier et al. (2000) in a ($Z-J$, Z) UKIDSS passbands colour–magnitude diagram, as shown in Fig. 1, i.e. none of them exhibit any substantial excess at these near-infrared wavelengths. The objects are also generally free from reddening caused by extinction (Dawson et al. 2011, also see Appendix A this paper). Consequently, it can be inferred that the ($Z-J$, Z) value for any of the objects is photospheric in origin with negligible contribution from any circumsubstellar disc. Thus, the method of selecting these 119 objects is unbiased with respect to the presence of circumsubstellar discs.

As pointed out above, the 26 objects in our sample with published spectra have been confirmed to be very low-mass members of UpSco. In addition, we have recently obtained spectra for 25 further objects from this sample; all of them are confirmed as very low mass members of UpSco as well (Dawson et al., in preparation). Although the spectroscopic follow-up is not yet complete for our sample, the 100 per cent success rate for almost half the sample indicates that our selection method based on photometry and proper motion generates a clean, unbiased sample with negligible contamination by background objects ($\leq$2 per cent).

3 *WISE* DATA

For 116 of the 119 targets discussed above we obtained *WISE* data. The remaining three were not listed in the *WISE* data base. For the 116, the 2MASS identifier listed in the *WISE* data base agrees with the one from UKIDSS. In addition, all objects were visually examined in the *WISE* images and in the UKIDSS images. It was found that for the 116 objects analysed here, the identification of the UKIDSS source with the *WISE* source at the same position is unambiguous (for the three excluded targets this is not the case). Furthermore, since our target fields are sparsely populated and well above the Galactic plane (latitude 10–30 deg), the likelihood of accidental contamination by other objects is very low.

WISE surveyed the whole sky in four mid-infrared wavebands simultaneously, using passbands with effective wavelengths of 3.4 ($W1$), 4.6 ($W2$), 12 ($W3$) and 22 μm ($W4$). We used the results of profile-fitting photometry from the All Sky Data Release, further details of which can be found in Cutri et al. (2012).[1] Among the 116 objects are 2 that were previously examined by Scholz et al. (2007) and confirmed to have discs.

[1] For more details of the *WISE* All Sky Data Release also see http://wise2.ipac.caltech.edu/docs/release/allsky/expsup/.

4 COLOUR ANALYSIS

The five United Kingdom Infrared Telescope (UKIRT) passbands; *Z*, *Y*, *J*, *H* and *K* have respective wavelengths of 0.88, 1.03, 1.25, 1.63 and 2.20 μm. Similar *J*, *H* and *K* passbands are also used in 2MASS. As noted above, the four *WISE* passbands, *W*1, *W*2, *W*3 and *W*4, have longer wavelengths of 3.4, 4.6, 12 and 22 μm, respectively. Different colour–colour and colour–magnitude diagrams using combinations of all nine passbands were examined. The ($Z-J$, Z) and ($W1$–$W2$,Z) colour–magnitude diagrams are shown in Fig. 1. Theoretical isochrones for 5 Myr old substellar objects are also shown overplotted on the diagrams. These isochrones are based on the DUSTY models derived by Chabrier et al. (2000) and obtained from both Baraffe and Allard (private communications). The isochrones were computed using both the UKIDSS and *WISE* filter profiles. The ($Z-J$, Z) isochrone was used to assign masses to objects by Dawson et al. (2011). The uppermost point on the 5 Myr isochrone corresponds to a mass of 0.09 $M_{\odot}$ while the lowest point corresponds to a mass of 0.01 $M_{\odot}$.

4.1 *WISE* data for UpSco brown dwarfs

4.1.1 W*1*−W*2 *(3.4–4.6 μm)*

In the ($Z-J$, Z) diagram all the objects are grouped close to the isochrone and none show any significant colour excess, as discussed above. However, two distinct populations of objects are clearly visible in the ($W1-W2$,Z) diagram, one close to the isochrone and one showing an excess in $W1-W2$ (3.4–4.6 μm). The population with excess is best understood as objects harbouring dusty discs and therefore emitting thermal infrared radiation (class II). These two populations do not show up in the diagrams that utilize only UKIRT passbands. Other diagrams that combine both UKIRT and *WISE* passbands do show the two populations. Colours that use a UKIRT and *WISE* *W*1 (3.4 μm) passband do show the two populations but not as clearly as colours incorporating *W*2 (4.6 μm). The $K-W2$ colour in particular discriminates between the two populations almost as well as the $W1-W2$ colour. The $W1-W2$ colour was chosen as the primary diagnostic for distinguishing between class II and class III objects in this work (see Figs 1 and 2).

4.1.2 W*1*−W*2*: *Comparison with Scholz et al. (2007)*

To test that the method outlined above was successfully discriminating between class II and class III objects, it was also applied to the 35 objects in UpSco examined by Scholz et al. (2007). That study used a *Spitzer* survey combining spectroscopy from 8 to 12 μm and photometry at 24 μm. As 33 of the 35 objects lie outside the area covered by UKIDSS there is no *Z* or *Y* passband data available for them. However, they are recorded in the *J*, *H* and *K* passbands of 2MASS. The 35 objects were plotted in a ($W1-W2$,J) colour–magnitude diagram (shown in the right-hand panel of Fig. 2) using data from 2MASS. The 116 objects from this work were also plotted in a ($W1-W2$,J) colour–magnitude diagram (shown in the left-hand panel of Fig. 2) for comparison, using data from the UKIDSS *J* passband. Two of the objects from Scholz et al. (2007) lie inside the area covered by UKIDSS and were recovered by Dawson et al. (2011). The differences in their UKIDSS and 2MASS *J* magnitudes are negligible (0.06 mag in both cases).

As can be seen from the right-hand panel of Fig. 2, all the objects with circumsubstellar discs have sufficient excess in $W1-W2$ (3.4–4.6 μm) to stand clear of the objects with no discs clustered along the isochrone. A few of the objects with discs exhibit a lesser, but still significant colour excess in $W1-W2$ (i.e. they are more than 2σ away from the isochrone). The method successfully discriminated between the 13 class II and 22 class III objects in this sample.

4.1.3 W*3 (12 μm)*

Colours that utilize the longer wavelength *W*3 (12 μm) passband are of limited use as only 39 of the 116 objects have an S/N > 5.0 in *W*3. By contrast, all 116 objects have an S/N > 8.0 in *W*1 and *W*2. The 39 objects with an S/N > 5.0 in *W*3 were further examined in the ($W1-W2$,$W3$) colour–magnitude diagram shown in Fig. 3. They are all among the higher mass objects in the sample, as evidenced by the lack of objects around the lower part of the isochrone. The population with the $W1-W2$ (3.4–4.6 μm) colour excess is again distinct from the population close to the isochrone as in the previous diagrams. The ninth brightest object in *W*3 now stands clear from the population near the isochrone. While this object is not obviously part of the population with excess in $W1-W2$ seen in Figs 1 and

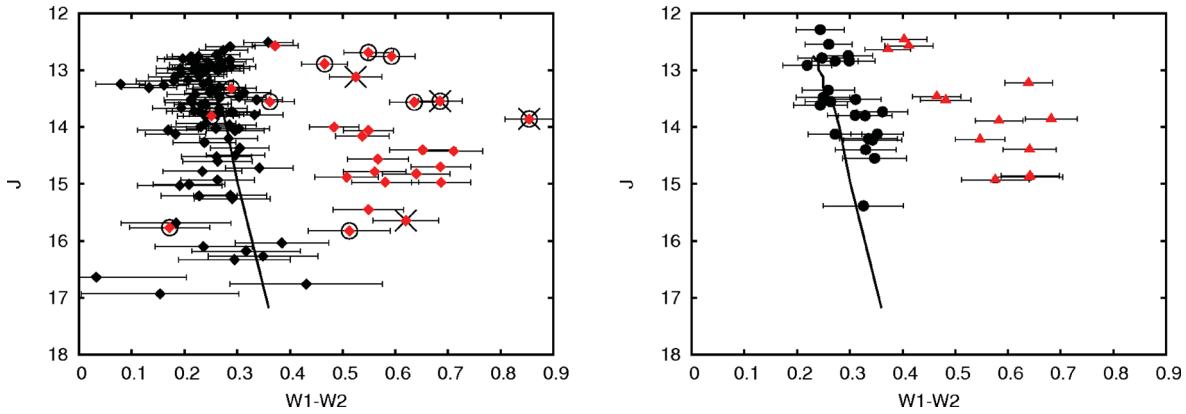

Figure 2. ($W1-W2$,J) colour–magnitude diagrams. The 116 brown dwarfs with available *WISE* data analysed in this work are shown in the left-hand panel with symbols and isochrone as in Fig. 1. The right-hand panel shows the same diagram for 35 objects in UpSco identified in Scholz et al. (2007). Objects confirmed as having discs in Scholz et al. (2007) are shown as closed triangles while those with no disc detected are shown as closed circles. As can be seen, the objects in the population with obvious colour excess all have discs. A few objects with discs exhibit a smaller, but still significant colour excess (i.e. they are more than 2σ away from the isochrone). Objects with no disc lie close to the isochrone.

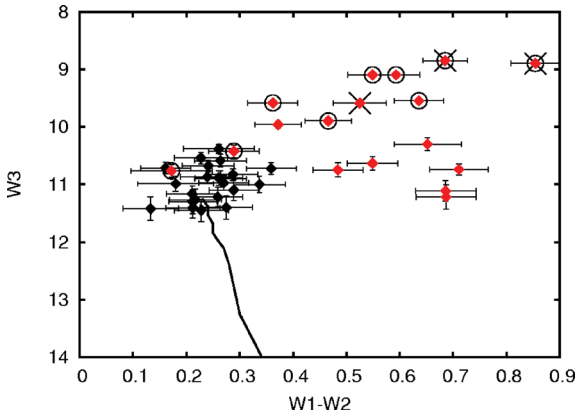

Figure 3. (*W*1−*W*2,*W*3) colour–magnitude diagram for 39 of the 116 objects with an S/N > 5.0 in *W*3 (12 μm). Symbols and isochrone are the same as in Fig. 1. The 39 objects are all among the higher mass objects in the sample, as evidenced by the lack of objects around the lower part of the isochrone.

2, it is more than 2σ away from the isochrone. On the combined basis of its excess in *W*1−*W*2 and its brightness in *W*3, it appears to have a disc and so is included in the group of class II objects. This object is one of the two objects common to both this study and that of Scholz et al. (2007) who note that it has a binary companion at a separation of 12 au.

4.1.4 W*4 (22 μm)*

The objects also had their detection in the *W*4 (22 μm) *WISE* passband examined. Photospheric emission from brown dwarfs is negligible by comparison with emission from a disc at wavelengths longer than 20 μm (Scholz et al. 2007). Therefore, any object with a bright unambiguous signal in *W*4 shows clear evidence of the presence of a dusty disc, even if it does not have an excess in *W*1−*W*2 (3.4–4.6 μm). 105 of the objects were not distinguishable from the background in *W*4, having S/N varying from 4.7 to 0. The remaining 11 were detected with S/N > 5.0 and have the brightest signals in *W*4. These 11 are marked with rings in Figs 1, 2, 3 and 4. Of the 11, 7 are in the population of 22 with distinct *W*1−*W*2 (3.4–4.6 μm) colour excess.

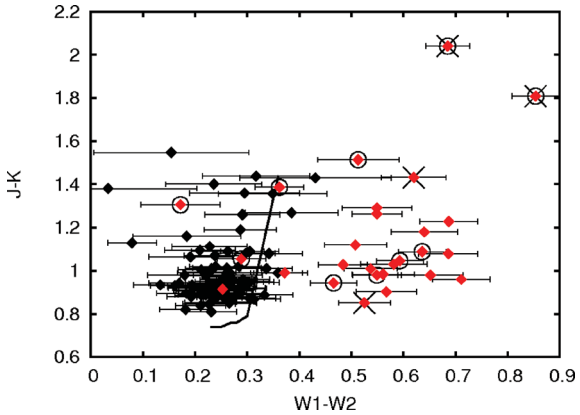

Figure 4. (*W*1−*W*2,*J* − *K*) colour–colour diagram with brown dwarfs and isochrones as in Figs 1 and 2. The two objects which are bright in *W*4 and which show signs of accretion have an excess in both *W*1−*W*2 and *J* − *K*. Apart from those two, the rest of the population with excess in *W*1−*W*2 shows no obvious excess in *J* − *K*.

Table 1. Objects with photometric variability >0.2 mag in *J*,*H* or *K*.

Name	Δ*J*	Δ*H*	Δ*K*
2MASS J15514709−2113234	0.84	0.59	0.25
2MASS J15521088−2125372	0.24	0.11	0.03
2MASS J15472282−2139141	0.38	0.25	0.21
2MASS J16030235−2626163	0.17	0.30	0.11

4.1.5 (W1−W2, J − K)

The (*W*1−*W*2, *J* − *K*) colour–colour diagram in Fig. 4 was examined to see if class II and class III objects could be clearly separated. Apart from the two objects which are bright in *W*4 and have large differences in their UKIDSS and 2MASS *J* magnitudes, none of the objects show any significant excess in *J* − *K*. This serves to confirm previous findings (Natta & Testi 2001; Natta et al. 2002) that the efficacy of using *J* − *K* excess as a diagnostic for the presence of discs around very low mass stars and brown dwarfs is very limited.

4.2 Variable objects

A comparison was also made of the UKIDSS and 2MASS photometry for each object. UKIDSS and 2MASS data were gathered at different epochs several years apart – 2MASS between 1997 and 2001 (Skrutskie et al. 2006) and UKIDSS from 2005 onwards (Lawrence et al. 2007). Of the 116 objects, 112 showed a variation of less than 0.2 mag in *J*, *H* and *K*. The remaining four, which are listed in Table 1 (and marked with crosses in Figs 1, 2, 3 and 4), showed variations of greater than 0.2 mag in *J*, *H* or *K*. Such variations in *J* have been interpreted by Scholz et al. (2009) as signatures of accretion. Scholz et al. (2009) further note that coolspots (comparable to sunspots) are expected to produce variations of <0.15 mag in *J* and <0.1 mag in *K* while large-scale photometric variability with amplitudes declining towards longer wavelengths – as displayed by the three most variable objects in Table 1 – is generally caused by hotspots or variable extinction due to a rotating disc. Hotspots in young stars and brown dwarfs are thought to be a direct consequence of accretion and so they are evidence of the existence of a disc. Likewise, variable extinction is also evidence of the existence of a disc. All four objects are in the population with *W*1−*W*2 colour excess.

5 DISCUSSION

In all, 22 objects were identified as class II objects on the basis of their *W*1−*W*2 colour alone. One object with a small *W*1−*W*2 excess was also placed in the population of class II objects because of its bright *W*3 signal. A further four other objects with no *W*1−*W*2 excess were also categorized as class II because of their bright signals in the 22 μm *W*4 passband. All 27 objects are listed in Table 2. The remaining 89 objects (listed in Table 3) were deemed to be class III, i.e. they have no discs or discs with a large inner opacity hole of at least 5–20 au (see Scholz et al. 2007). We show the spectral energy distributions for six characteristic examples of the class II objects in Appendix B.

5.1 Disc fraction

The overall disc fraction is 27 out of 116 or 23 ± 5 per cent (the uncertainty corresponds to a 1σ confidence interval based on binomial statistics). As noted in Section 2 above, contamination in

Table 2. Positions, UKIDSS *Z* and *J* photometry, *WISE W*1, *W*2, *W*3 and *W*4 photometry of the 27 class II objects. Objects are listed in order of decreasing mass, based on their Z magnitude. Coordinates are J2000.

Name	RA	Dec.	*Z* Mag.	*J* Mag.	*W*1 Mag.	*W*2 Mag.	*W*3 Mag.	*W*4 Mag.
2MASS J16075049−2125200	16:07:50.49	−21:25:20.2	14.03	12.69	11.27	10.73	9.10	7.22
2MASS J15465432−2556520	15:46:54.32	−25:56:52.1	14.16	12.75	11.40	10.81	9.10	6.23
2MASS J16052875−2655496	16:05:28.75	−26:55:49.7	14.18	12.89	11.67	11.21	9.90	8.03
2MASS J16095852−2345186	16:09:58.52	−23:45:18.7	14.20	12.57	11.34	10.97	9.96	8.73[a]
2MASS J16030235−2626163	16:03:02.36	−26:26:16.4	14.46	13.12	11.44	10.92	9.59	8.04[a]
2MASS J15470374−2601183	15:47:03.74	−26:01:18.4	15.02	13.32	12.03	11.74	10.42	7.39
2MASS J16134880−2509006	16:13:48.81	−25:09:00.7	15.04	13.56	11.96	11.32	9.55	7.58
2MASS J15514709−2113234	15:51:47.09	−21:13:23.5	15.12	13.54	10.56	9.88	8.85	7.41
2MASS J16035573−2738248	16:03:55.73	−27:38:25.1	15.19	13.80	12.70	12.45	12.13[a]	7.89
2MASS J15472572−2609185	15:47:25.73	−26:09:18.5	15.40	13.55	11.87	11.51	9.58	7.37
2MASS J16145253−2718557	16:14:52.53	−27:18:55.7	15.65	14.06	12.34	11.79	10.63	8.70[a]
2MASS J15412655−2613253	15:41:26.55	−26:13:25.4	15.65	14.00	12.59	12.10	10.75	8.24[a]
2MASS J15521088−2125372	15:52:10.88	−21:25:37.4	15.72	13.86	11.01	10.15	8.90	6.92
2MASS J16143287−2242133	16:14:32.87	−22:42:13.5	15.82	14.16	12.88	12.34	11.74[a]	8.38[a]
2MASS J15501958−2805237	15:50:19.58	−28:05:23.9	16.04	14.56	13.28	12.72	12.03[a]	8.98[a]
2MASS J16080745−2345055	16:08:07.45	−23:45:05.6	16.06	14.40	12.86	12.21	10.30	8.43[a]
2MASS J15524513−2705560	15:52:45.13	−27:05:56.1	16.16	14.42	13.06	12.35	10.74	8.66[a]
2MASS J15571880−2711567	15:57:18.81	−27:11:56.8	16.39	14.78	13.42	12.86	11.90[a]	9.05[a]
2MASS J16142144−2339146	16:14:21.44	−23:39:14.8	16.59	14.97	13.57	12.99	11.95[a]	8.25[a]
2MASS J16012238−2708194	16:01:22.39	−27:08:19.5	16.68	14.70	13.24	12.55	11.11	8.43[a]
2MASS J16100608−2127440	16:10:06.08	−21:27:44.1	16.82	14.82	13.29	12.65	11.90[a]	8.72[a]
2MASS J15541998−2135428	15:54:19.99	−21:35:43.0	16.85	14.98	13.26	12.57	11.22	8.39[a]
2MASS J16083048−2335109	16:08:30.49	−23:35:11.0	16.95	14.88	13.37	12.86	11.69[a]	8.63[a]
2MASS J16082847−2315103	16:08:28.47	−23:15:10.4	17.64	15.45	13.77	13.22	12.21[a]	8.34[a]
2MASS J15472282−2139141	15:47:22.82	−21:39:14.3	17.97	15.65	13.69	13.07	11.63[a]	8.67[a]
2MASS J15433947−2535549	15:43:39.47	−25:35:54.9	18.15	15.77	13.91	13.73	10.77	7.78
2MASS J15553614−2546591	15:55:36.15	−25:46:59.2	18.23	15.83	13.63	13.12	11.10[a]	7.92

[a]S/N < 5.

Table 3. Positions, UKIDSS *Z* and *J* photometry, *WISE W*1, *W*2, *W*3 and *W*4 photometry of the 89 class III objects. Objects are listed in order of decreasing mass, based on their *Z* magnitude. Coordinates are J2000.

Name	RA	Dec.	*Z* Mag.	*J* Mag.	*W*1 Mag.	*W*2 Mag.	*W*3 Mag.	*W*4 Mag.
2MASS J16175608−2856399	16:17:56.09	−28:56:40.0	14.01	12.76	11.76	11.53	10.54	8.17[a]
2MASS J16034797−2801319	16:03:47.97	−28:01:31.9	14.03	12.81	11.83	11.62	11.17	9.02[a]
2MASS J16105728−2359540	16:10:57.28	−23:59:54.1	14.04	12.80	11.68	11.48	11.72[a]	8.72[a]
2MASS J15554229−2546477	15:55:42.29	−25:46:47.8	14.07	12.65	11.52	11.24	10.93[a]	8.18[a]
2MASS J16055898−2556228	16:05:58.99	−25:56:22.9	14.10	12.59	11.50	11.22	10.83	9.08[a]
2MASS J16105429−2309108	16:10:54.29	−23:09:11.1	14.13	12.97	11.88	11.68	11.60[a]	8.27[a]
2MASS J15591513−2840411	15:59:15.12	−28:40:41.3	14.14	12.96	12.00	11.77	12.39[a]	8.75[a]
2MASS J16095217−2136277	16:09:52.17	−21:36:27.8	14.15	12.51	11.33	10.97	10.72	9.14[a]
2MASS J16063691−2720548	16:06:36.91	−27:20:54.9	14.16	12.88	11.85	11.60	11.91[a]	8.73[a]
2MASS J15411513−2539447	15:41:15.14	−25:39:44.8	14.16	12.76	11.59	11.37	11.30	8.71[a]
2MASS J16033799−2611544	16:03:37.99	−26:11:54.4	14.17	12.98	11.96	11.70	11.22	8.63[a]
2MASS J16105499−2126139	16:10:54.99	−21:26:14.0	14.22	12.73	11.56	11.30	10.89	8.53[a]
2MASS J16154869−2710546	16:15:48.69	−27:10:54.7	14.22	12.82	11.69	11.40	11.65[a]	8.86[a]
2MASS J15450519−2559047	15:45:05.20	−25:59:04.7	14.23	12.90	11.76	11.54	12.00[a]	8.53[a]
2MASS J16072196−2358452	16:07:21.96	−23:58:45.3	14.24	12.99	11.86	11.64	11.27	8.79[a]
2MASS J16152819−2315439	16:15:28.19	−23:15:44.1	14.24	13.12	12.08	11.90	11.78[a]	8.18[a]
2MASS J16370523−2625439	16:37:05.24	−26:25:44.0	14.27	12.96	11.96	11.69	11.40	8.91[a]
2MASS J15492909−2815384	15:49:29.08	−28:15:38.6	14.29	12.96	11.85	11.63	12.05[a]	8.91[a]
2MASS J15491602−2547146	15:49:16.02	−25:47:14.6	14.31	13.01	11.87	11.60	10.90	8.20[a]
2MASS J16082229−2217029	16:08:22.29	−22:17:03.0	14.31	12.94	11.85	11.56	11.10	8.81[a]
2MASS J16061595−2218279	16:06:15.95	−22:18:28.0	14.31	13.17	12.11	11.91	11.92[a]	9.02[a]
2MASS J15544260−2626270	15:54:42.61	−26:26:27.0	14.32	13.05	11.91	11.72	11.61[a]	8.23[a]
2MASS J16090168−2740521	16:09:01.68	−27:40:52.3	14.33	12.86	11.71	11.44	10.97	8.72[a]
2MASS J15582376−2721435	15:58:23.76	−27:21:43.7	14.35	13.07	12.02	11.79	11.37[a]	8.78[a]
2MASS J16132180−2731219	16:13:21.80	−27:31:22.0	14.36	13.25	11.93	11.85	11.60[a]	8.77[a]
2MASS J15415562−2538465	15:41:55.63	−25:38:46.5	14.37	13.10	12.02	11.79	12.14[a]	8.93[a]
2MASS J16002535−2644060	16:00:25.35	−26:44:06.1	14.38	13.02	11.90	11.66	11.67[a]	8.50[a]

Table 3 – *continued*

Name	RA	Dec.	*Z* Mag.	*J* Mag.	*W*1 Mag.	*W*2 Mag.	*W*3 Mag.	*W*4 Mag
2MASS J15545410−2114526	15:54:54.11	−21:14:52.7	14.40	13.26	12.10	11.94	10.71	8.31[a]
2MASS J16062637−2306113	16:06:26.37	−23:06:11.4	14.48	13.20	12.12	11.87	11.68[a]	8.90[a]
2MASS J16121609−2344248	16:12:16.09	−23:44:25.0	14.50	13.19	11.96	11.78	10.99	8.21[a]
2MASS J16090451−2224523	16:09:04.51	−22:24:52.5	14.57	12.92	11.66	11.40	10.59	8.23[a]
2MASS J16113470−2219442	16:11:34.70	−22:19:44.3	14.61	13.24	12.11	11.87	12.25[a]	8.77[a]
2MASS J15505993−2537116	15:50:59.94	−25:37:11.7	14.62	13.33	12.30	12.05	11.55[a]	8.90[a]
2MASS J15524857−2621453	15:52:48.57	−26:21:45.4	14.62	13.30	12.27	12.00	12.51[a]	9.14[a]
2MASS J16372782−2641406	16:37:27.83	−26:41:40.7	14.63	13.30	12.14	12.00	11.42	8.95[a]
2MASS J15522943−2721003	15:52:29.44	−27:21:00.4	14.64	13.47	12.45	12.14	12.36[a]	9.06[a]
2MASS J15530374−2600306	15:53:03.75	−26:00:30.7	14.66	13.43	12.36	12.14	12.03[a]	8.62[a]
2MASS J15493660−2815141	15:49:36.59	−28:15:14.3	14.66	13.39	12.36	12.05	11.63[a]	8.79[a]
2MASS J16133476−2328156	16:13:34.76	−23:28:15.7	14.74	13.48	12.39	12.12	11.77[a]	8.81[a]
2MASS J15490803−2839550	15:49:08.02	−28:39:55.2	14.82	13.60	12.45	12.21	10.68	8.15[a]
2MASS J16112630−2340059	16:11:26.30	−23:40:06.1	14.83	13.40	12.16	11.92	12.04[a]	8.55[a]
2MASS J15495733−2201256	15:49:57.33	−22:01:25.7	14.89	13.35	12.15	11.89	11.56[a]	8.64[a]
2MASS J16062870−2856580	16:06:28.70	−28:56:58.2	14.90	13.52	12.39	12.18	11.41	9.06[a]
2MASS J15572692−2715094	15:57:26.93	−27:15:09.5	14.93	13.66	12.59	12.39	12.00[a]	9.10[a]
2MASS J16164539−2333413	16:16:45.39	−23:33:41.6	14.99	13.73	12.62	12.33	11.61[a]	8.44[a]
2MASS J16005265−2812087	16:00:52.66	−28:12:09.0	15.04	13.57	12.48	12.27	11.79[a]	9.13[a]
2MASS J16132665−2230348	16:13:26.66	−22:30:35.0	15.05	13.52	12.33	11.99	11.00	8.82[a]
2MASS J16115737−2215066	16:11:57.37	−22:15:06.8	15.07	13.67	12.51	12.24	11.76[a]	8.84[a]
2MASS J16064910−2216382	16:06:49.10	−22:16:38.4	15.09	13.73	12.63	12.37	11.90[a]	8.79[a]
2MASS J15585793−2758083	15:58:57.93	−27:58:08.5	15.13	13.81	12.78	12.54	12.08[a]	9.06[a]
2MASS J15420830−2621138	15:42:08.31	−26:21:13.8	15.15	13.74	12.59	12.32	12.10[a]	9.07[a]
2MASS J16090197−2151225	16:09:01.98	−21:51:22.7	15.16	13.59	12.32	12.08	10.87	8.45[a]
2MASS J16124692−2338408	16:12:46.92	−23:38:40.9	15.18	13.60	12.42	12.19	12.20[a]	8.25[a]
2MASS J16153648−2315175	16:15:36.48	−23:15:17.6	15.19	13.93	12.85	12.61	12.03[a]	8.23[a]
2MASS J16134264−2301279	16:13:42.64	−23:01:28.0	15.19	13.72	12.47	12.25	12.20[a]	8.38[a]
2MASS J16113837−2307072	16:11:38.37	−23:07:07.5	15.19	13.74	12.60	12.31	11.97[a]	8.59[a]
2MASS J15583403−2803243	15:58:34.03	−28:03:24.5	15.21	13.72	12.53	12.30	11.45	9.03[a]
2MASS J16192399−2818374	16:19:23.99	−28:18:37.5	15.29	13.79	12.73	12.40	11.51[a]	8.57[a]
2MASS J15490414−2120150	15:49:04.14	−21:20:15.2	15.31	13.77	12.64	12.37	11.50[a]	8.92[a]
2MASS J16051243−2624513	16:05:12.43	−26:24:51.4	15.40	14.06	12.93	12.76	12.29[a]	9.08[a]
2MASS J15533067−2617307	15:53:30.68	−26:17:30.7	15.49	13.99	12.83	12.60	12.06[a]	8.64[a]
2MASS J15544486−2843078	15:54:44.85	−28:43:07.9	15.51	14.12	12.99	12.81	12.60[a]	8.90[a]
2MASS J15531698−2756369	15:53:16.98	−27:56:37.2	15.53	13.96	12.84	12.55	12.50[a]	8.58[a]
2MASS J15551960−2751207	15:55:19.59	−27:51:21.0	15.60	14.03	12.93	12.67	12.30[a]	9.10[a]
2MASS J15564227−2646467	15:56:42.28	−26:46:46.8	15.62	14.03	12.85	12.54	11.65[a]	8.51[a]
2MASS J16101316−2856308	16:10:13.15	−28:56:31.0	15.67	14.06	12.89	12.59	12.16[a]	9.09[a]
2MASS J16115439−2236491	16:11:54.39	−22:36:49.3	15.73	14.27	13.04	12.80	11.86[a]	8.32[a]
2MASS J16092938−2343121	16:09:29.39	−23:43:12.2	15.96	14.20	12.94	12.65	12.30[a]	8.98[a]
2MASS J16103014−2315167	16:10:30.14	−23:15:16.8	16.06	14.37	13.05	12.75	11.97[a]	8.35[a]
2MASS J15561721−2638171	15:56:17.21	−26:38:17.2	16.10	14.52	13.26	13.00	10.38	8.23[a]
2MASS J16072641−2144169	16:07:26.41	−21:44:17.1	16.17	14.60	13.43	13.17	12.26[a]	8.55[a]
2MASS J16142061−2745497	16:14:20.61	−27:45:49.8	16.31	14.49	13.22	12.93	12.26[a]	8.69[a]
2MASS J15572820−2708430	15:57:28.21	−27:08:43.0	16.40	14.78	13.71	13.47	12.21[a]	8.77[a]
2MASS J16134079−2219459	16:13:40.79	−22:19:46.1	16.49	14.72	13.42	13.08	12.05[a]	8.99[a]
2MASS J15442275−2136092	15:44:22.75	−21:36:09.3	16.55	15.01	13.69	13.48	11.68[a]	8.55[a]
2MASS J15543065−2536054	15:54:30.65	−25:36:05.5	16.73	15.03	13.80	13.61	11.58[a]	8.17[a]
2MASS J16064818−2230400	16:06:48.18	−22:30:40.1	16.82	14.93	13.63	13.37	12.04[a]	8.68[a]
2MASS J15444172−2619052	15:44:41.72	−26:19:05.3	17.16	15.21	13.86	13.63	12.26[a]	8.86[a]
2MASS J16072382−2211018	16:07:23.82	−22:11:02.0	17.24	15.20	13.70	13.41	12.20[a]	8.87[a]
2MASS J16104714−2239492	16:10:47.13	−22:39:49.4	17.44	15.26	13.80	13.51	12.02[a]	8.57[a]
2MASS J16084744−2235477	16:08:47.44	−22:35:47.9	17.74	15.69	14.30	14.11	12.28[a]	8.79[a]
2MASS J15491331−2614075	15:49:13.32	−26:14:07.5	18.29	16.04	14.50	14.12	12.16[a]	8.88[a]
2MASS J16081843−2232248	16:08:18.43	−22:32:25.0	18.51	16.10	14.28	14.05	11.56[a]	8.72[a]
2MASS J16195827−2832276	16:19:58.26	−28:32:27.8	18.74	16.18	14.42	14.10	12.47[a]	8.77[a]
2MASS J15451990−2616529	15:45:19.91	−26:16:53.0	18.77	16.27	14.41	14.06	11.85[a]	8.20[a]
2MASS J16362646−2720024	16:36:26.47	−27:20:02.5	18.77	16.33	14.52	14.22	11.44[a]	8.79[a]
2MASS J16360175−2703305	16:36:01.75	−27:03:30.5	19.12	16.64	14.95	14.91	12.07[a]	8.86[a]
2MASS J16073799−2242468	16:07:37.99	−22:42:47.0	19.24	16.76	15.16	14.73	12.51[a]	8.25[a]
2MASS J15504498−2554213	15:50:44.99	−25:54:21.4	19.90	16.93	14.86	14.70	11.84[a]	8.33[a]

[a]S/N < 5.

our sample appears to be negligible. Conservatively assuming that 10 per cent of the objects are contaminants which do not exhibit mid-infrared excess would only increase the disc fraction to 27/104, i.e. 26 per cent. This contrasts with the previous results for UpSco of 37 ± 9 per cent (Scholz et al. 2007) obtained with a smaller sample of 35 objects. The sample of 35 objects in Scholz et al. (2007) was selected from the surveys of (Ardila, Martin & Basri 2000, 12 objects) and (Martin et al. 2004, 23 objects). The higher disc fraction reported in Scholz et al. (2007) may be the result of using a smaller sample of objects or of a possible bias.

The results of Scholz et al. (2007) were also in contrast to the disc fraction of 19 per cent for K0–M5 stars in the same region obtained by Carpenter et al. (2006) using a sample of 127 K0–M5 stars. Our new result, of 23 ± 5 per cent, from a similarly sized sample of 116 objects, is statistically indistinguishable from the result of Carpenter et al. (2006), suggesting that disc lifetimes in UpSco for objects later than K0 show no dependence on the mass of the central object. We note that from our sample of 27 discs, 22 (from 72, 31 per cent) are found to be in the mass range 0.01–0.05 $M_{\odot}$, while only 5 (from 44, 11 per cent) are in the mass range 0.05–0.09 $M_{\odot}$. This may indicate a trend towards higher disc fractions for very low mass brown dwarfs, but it is not sufficiently robust to warrant further discussion.

5.1.1 *Disc fractions in other clusters*

This result for UpSco can be compared with those for Cha I (Luhman et al. 2005; Damjanov et al. 2007), IC 348 (Luhman et al. 2005; Lada et al. 2006) and σ Ori (Hernandez et al. 2007), three other associations for which similar information is available. Damjanov et al. (2007) report a disc fraction of 52 ± 6 per cent from a sample of 81 K3–M8 objects in Cha I, while Luhman et al. (2005) find a disc fraction of 50 ± 17 per cent from a much smaller sample of 18 objects later than M6. Luhman et al. (2005) also find a disc fraction of 42 ± 13 per cent for 24 objects later than M6 in IC 348, where Lada et al. (2006) report a disc fraction of 47 ± 12 per cent in the range of K6–M2 stars. In an analysis of discs in σ Ori, Hernandez et al. (2007) find a disc fraction of 36 ± 4 per cent for stars in the mass range 0.1–1.0 $M_{\odot}$ and 33 ± 10 per cent for brown dwarfs (defined as objects <0.1 $M_{\odot}$). The spectral types of the most massive stars in this range defined by Hernandez et al. (2007) are a little earlier than K (up to G8). However, the vast bulk of their sample is in the mass range of K and M stars, so their result is noted here as being valid for K and M stars in σ Ori. Fig. 5 shows that in the wake of this revision of the results for UpSco, all four associations now show similar disc fractions for K/M stars and brown dwarfs. Thus, average disc lifetime does not appear to be dependent on the mass of the central object in any of these regions.

5.1.2 *The ages of the associations*

All the associations listed above are young, i.e. <10 Myr old. Preibisch et al. (2002) determined an age of about 5 Myr for UpSco, while a revised age of 10 Myr has been proposed by Pecaut et al (2012). Cha I, IC 348 and σ Ori have each had various ages of between 2 and 5 Myr reported for each of them (Oliveira et al. 2002; Zaptero Osorio et al. 2002; Luhman et al. 2003; Luhman 2004, 2007; Sherry, Walter & Wolk 2004; Mayne et al. 2007). So while UpSco appears to be the oldest of the four associations, Cha I, IC 348 and σ Ori cannot yet be readily distinguished in terms of their ages. Ergo, apart from stating that the oldest association has the smallest disc fraction, no robust correlation can be safely determined in respect of the disc fractions and ages of the four associations.

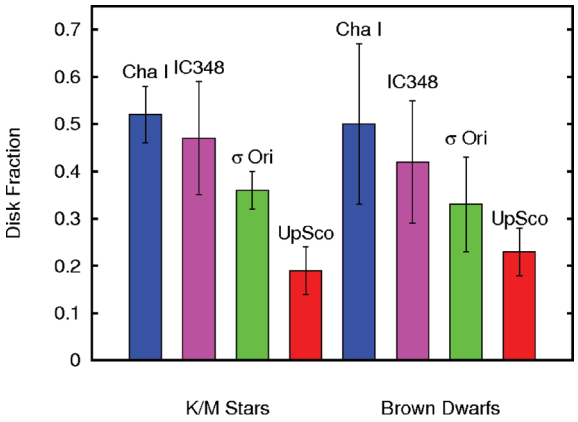

Figure 5. Disc fractions for K/M stars compared to disc fractions for brown dwarfs in Cha 1, IC 348, σ Ori and UpSco. In each case the disc fraction for the K/M stars is statistically indistinguishable from the disc fraction for the brown dwarfs (see the text; Section 5.1).

5.2 Transition discs

Objects with very little or no excess at near- to mid-infrared wavelengths but exhibiting excess at longer wavelengths are best understood by assuming an opacity hole in the inner disc (see Section 5.3). They may be in the process of clearing dust from their inner discs (Calvet et al. 2002; Muzerolle et al. 2006). Such objects are often termed 'transition discs', but the criteria used to define transition discs differ in the literature (see Merin et al. 2010; Luhman & Mamajek 2012 for a discussion of the various criteria). Here we use the term to identify objects with little or no excess in $W1-W2$, i.e. shortwards of 10 μm, but bright $W3$ and/or $W4$ signals (see Sections 4.1.3 and 4.1.4). The five objects that satisfy this criterion are included in the class II group and may be in the process of transition from class II to class III.

We do not find any object that might be called a 'pre-transitional disc' (Espaillat et al. 2008, 2012), showing evidence for an opacity gap (as opposed to an inner hole) in the disc, i.e. with excess at <10 μm, no excess at 12 μm and excess again at 22 μm.

Based on our adopted definition, the fraction of transition discs around class II brown dwarfs in our sample is 5/27 or 19 per cent. Due to the small sample size, the uncertainty in this number is in the range of ± 10 per cent. Taking this into account, the value is consistent with most previous estimates for the transition disc fraction for low-mass stars which are, for criteria similar to the one adopted here, in the range 0–20 per cent (e.g. Ercolano, Clarke & Robitaille 2009; Muzerolle et al. 2010). Thus, based on our estimate for the brown dwarf regime, there is no evidence for mass dependence in the transition disc frequency.

The small number of transition discs in our sample indicates that the transition phase lasts only a short time compared with the total lifetime of the discs. Assuming the upper limit for the age spread of 2 Myr (Preibisch & Zinnecker 1999), we obtain an upper limit of 0.4 Myr for the transition time-scale, i.e. about one order of magnitude shorter than the disc lifetime. Thus, a two time-scale model for the evolution of the discs, as often adopted for low-mass stars, is required for brown dwarfs as well.

5.3 Radiative transfer models

Scholz et al. (2007) produced model spectral energy distributions based on Monte Carlo radiative transfer simulations for the 13 class II objects that they found in UpSco. Fig. 6 shows the spectral energy distributions of the two of those objects recovered in this work, which have been recreated using the original model parameters. Data shown for the *J*, *H*, *K*, 9, 10, 11 and 24 μm wavelengths are taken from that of Scholz et al. (2007). The new data for the *W*1, *W*2 and *W*3 passbands are also shown overplotted on the two spectral energy distribution diagrams. It is clear from Fig. 6 that the data for *W*1 (3.4 μm), *W*2 (4.6 μm) and *W*3 (12 μm) agree very well with both original models, lying on or very close to the modelled flux for a combined photosphere and disc (solid lines in Fig. 6).

Models of the inner part of a disc rely on observational data in the mid-infrared to refine their accuracy. Scholz et al. (2007) noted that the gap in their data coverage in the 3–8 μm region restricted their ability to constrain the size of any inner disc holes in sources that exhibited excesses at 9 μm and beyond. The addition of the *W*1 and *W*2 data points for the two objects in Fig. 6 now allows the accuracy of the models in this region to be probed.

The data for the object in the left-hand panel was originally fitted with a model which included an excess in the mid-infrared which necessitated the presence of an optically thick inner disc. The newly overplotted *W*1 (3.4 μm) and *W*2 (4.6 μm) values observed by *WISE* conform with that part of the model, further indication that a significant *W*1-*W*2 excess is evidence for the presence of a disc. The $W1-W2$ excess for this object places it more than 4σ away from the isochrone in the ($W1-W2$,*Z*) colour–magnitude diagram in Fig. 1.

The diagram in the right-hand panel of Fig. 6 is for the object noted in Sections 4.1.3 and 5.2 above that may be in the process of transition from class II to class III. Its lesser excess at *W*1 and *W*2 is clear, as is its relatively greater excess at *W*3. Again, the accuracy of the original model at these wavelengths is confirmed by the newly observed *WISE* values. While the model shown does preclude the existence of an optically thick inner disc, it does not require the presence of an evacuated hole in the inner disc. Instead, a reduced scaleheight, i.e. a flatter inner disc is sufficient. This evolution to a flatter disc could be caused by grain growth and dust settling along the lines proposed by Dullemond & Dominik (2004). Ergo, in this model, the process of transition from class II to class III that may be occurring around this object's disc does not require the presence of mechanisms (e.g. planet formation) that would completely clear the inner disc.

5.4 Comparison with Riaz et al. (2012)

In a recent paper, Riaz et al. (2012) analyse a sample of 43 spectroscopically confirmed very low mass members (spectral types M4–M8.5) in UpSco using *WISE* data. They find six new class II objects and recover four others previously recorded by Scholz et al. (2007) and a further two that were found by Slesnick, Hillenbrand & Carpenter (2008). These 12 objects are listed in their table 1. We have been kindly provided with a table which includes the 31 other brown dwarfs that they investigated and categorized as class III by Riaz (private communication). From the 12 class II and 31 class III objects that they list, there are 12 in common to both that study and ours. Both studies categorize the same five objects as class II and the same seven objects as class III.

Also included in the table supplied by Riaz are six other objects with S/N <3.0 in the *W*3 passband. Riaz et al. (2012) rely on the use of the *W*3 signal and require that a source have a *W*3 S/N of ≥ 3.0. As a result they do not categorize these six brown dwarfs. However, using the $W1-W2$ colour as a primary diagnostic instead of *W*3 allows a larger range of objects to be successfully examined. All 116 objects investigated in our work have an S/N > 8 in the *W*1 and *W*2 passbands, while only 64 of them have an S/N of ≥ 3.0 in the *W*3 passband. The six objects which cannot be categorized in Riaz et al. (2012) because they have a weak *W*3 signal have been determined in this work to be class III objects using their *W*1 and *W*2 signals alone.

Requiring that a source have a *W*3 S/N of ≥ 3.0 not only restricts the number of objects in any sample from UpSco, but also produces a sample that is biased with respect to the presence of discs. Class III objects in UpSco are less likely than class II objects to have a strong *W*3 signal. Of the 116 objects examined in this work, 78 per cent of the class II objects, but only 48 per cent of the class III objects, have a *W*3 S/N of ≥ 3.0. Restricting the analysis to those 64 objects only would have yielded an artificially high disc fraction of 33 per cent, rather than the 23 per cent found from the larger unbiased sample

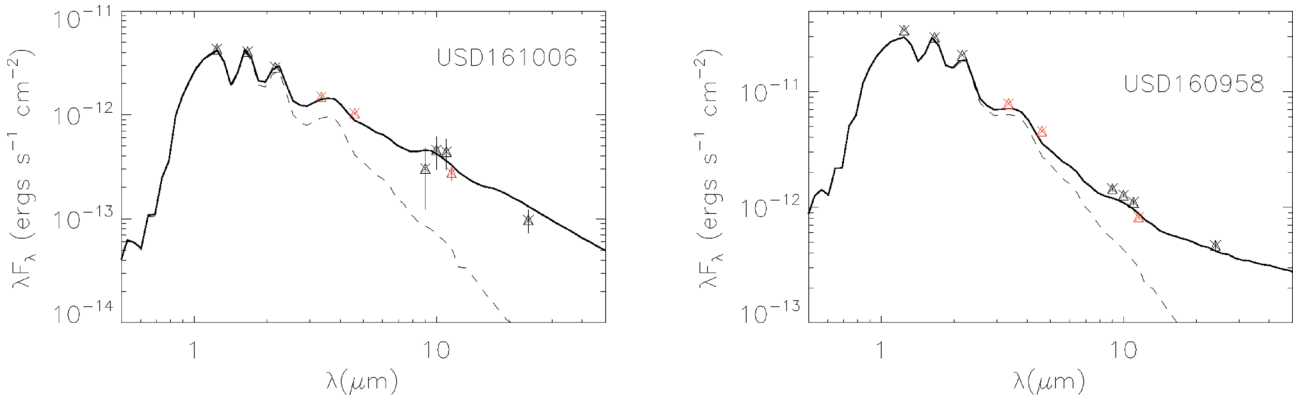

Figure 6. Spectral energy distribution for the two class II objects originally identified in Scholz et al. (2007) and recovered in this work. Data shown are taken from that of Scholz et al. (2007) for the *J*, *H*, *K*, 9, 10, 11 and 24 μm wavelengths, along with the newly acquired *W*1, *W*2 and *W*3 values. The Monte Carlo radiative transfer simulations shown for comparison use the same parameters as were given in Scholz et al. (2007). The dotted lines depict calculated photospheric flux while the solid lines represent combined photospheric and disc flux.

of 116 objects, while also increasing the statistical errors. For these reasons our disc fraction is a more representative value for the brown dwarf population in UpSco.

5.5 Comparison with Luhman & Mamajek 2012

Another recent paper focused on the discs of UpSco members has been published by Luhman & Mamajek (2012). Similar to Riaz et al. (2012) they look at a sample of spectroscopically confirmed members. Their list of targets includes 387 objects with spectral types M4–M8 and another 23 with M8–L2 and is thus substantially larger than the Riaz et al. sample. They analyse the available *Spitzer* and *WISE* photometry for these objects. To identify the objects with discs, they use the spectral regime from 4.5 to 24 μm, similar to this paper.

48 of their targets also appear in our total sample of 119, among them 13 classified as class II in this paper. In most cases, our class II/III distinction agrees with the one in Luhman & Mamajek (2012). The only exception is the M9–L1 object 2MASSJ 16082847−2315103, which clearly fulfils our class II criterion based on its $W1-W2$ colour, whereas Luhman & Mamajek (2012) conclude that it is diskless based on its $K-W2$ colour. At these late spectral types, however, the intrinsic colours of young brown dwarfs increase significantly with spectral type and cover a broad range, i.e. it is challenging to unambiguously distinguish between class II and class III. Whether this source does or does not have infrared excess emission remains to be determined, but this does not affect our results in any way.

The remainder of our sample (71 in total, among them 14 with discs) is new and not covered by Luhman & Mamajek (2012), i.e. our work increases the sample of brown dwarfs analysed with mid-infrared data significantly.

The disc fraction derived by Luhman & Mamajek (2012) for very low mass and substellar members of UpSco is ∼25 per cent, and thus agrees very well with our own result. They also find that disc fractions increase from very small values for B–G stars (≤10 per cent) to 25 per cent for ≥M5 objects. This seems at odds with our own statement of spectral type-independent disc fractions, but a more detailed examination shows that the two studies actually give consistent results for K and M stars.

Luhman & Mamajek (2012) report disc fractions of 6/67 for K0–M0, 35/231 for M0–M4, 97/387 for M4–M8 and 4/23 for M8–L2. To compare with our own values, we calculated the binomial confidence intervals for their disc fractions and obtain 14 ± 3 per cent for K0–M4 and 25 ± 3 per cent for M4–L2. This is consistent with the numbers quoted in Section 5.1. (19 per cent for K0–M5 and 23 per cent for our sample of brown dwarfs). Note that the uncertainties quoted above only give the statistical confidence interval and do not take into account possible biases (e.g. age spread across the region, uncertainties in spectral types). Thus, based on the current samples, the evidence for a mass dependence of the disc fraction for objects later than K0 is marginal at best.

6 CONCLUSIONS

We have carried out a survey for discs around a homogeneous sample of 119 brown dwarfs, the majority of which have not been previously discussed in the literature, in the 5 Myr old UpSco star-forming region using photometry from *WISE*. Contamination in the sample appears to be negligible and the method of selection is unbiased with respect to the presence of discs.

Examining all the UKIDSS, 2MASS and *WISE* colour–magnitude and colour–colour combinations shows that the *WISE* $W1-W2$ colour is the best primary diagnostic for the presence of a disc around the objects.

27 class II objects are identified from the sample. 22 were classified via their $W1-W2$ colour excess alone. Five other objects were also categorized as class II from their $W3$ and/or $W4$ signals. These five objects (19 per cent of all discs) appear to be in the transition phase between class II and class III, leading to the conclusion that this phase is short lived, lasting less than 0.4 Myr, an estimate that is consistent with findings for low-mass stars.

The disc fraction is found to be 23 ± 5 per cent. This fraction is statistically indistinguishable from results for K/M stars in UpSco. Results from the literature for Cha I, IC 348 and σ Ori show that their brown dwarf disc fractions are also indistinguishable from their K/M star disc fractions. Therefore, the average lifetime of the discs in each of these regions shows no obvious dependence on the mass of the central object. Combined with the short transitional phase from class II to class III, this suggests that the evolution of brown dwarf discs follows 'a two time-scale model', similar to low-mass stars.

ACKNOWLEDGMENTS

The authors would like to thank Isabelle Baraffe of Exeter University and France Allard of the Centre de Recherche Astrophysique de Lyon for supplying model data. This work was supported by Science Foundation Ireland within the Research Frontiers Programme under grant no. 10/RFP/AST2780. This publication makes use of data products from the *WISE*, which is a joint project of the University of California, Los Angeles, and the Jet Propulsion Laboratory/California Institute of Technology, funded by the National Aeronautics and Space Administration. This publication also makes use of data products from the Two Micron All Sky Survey, which is a joint project of the University of Massachusetts and the Infrared Processing and Analysis Center/California Institute of Technology, funded by the National Aeronautics and Space Administration and the National Science Foundation. We would also like to thank the UKIDSS Team for the excellent data base they have made available to the community.

REFERENCES

Ardila D., Martin E., Basri G., 2000, AJ, 120, 479
Calvet N., D'Alessio P., Hartmann L., Wilner D., Walsh A., Sitko M., 2002, ApJ, 568, 1008
Carpenter J. M., Mamajek E. E., Hillenbrand L. A., Meyer M. R., 2006, ApJ, 651, L49
Chabrier G., Baraffe I., Allard F., Hauschildt P., 2000, ApJ, 542, 464
Cutri R. M. et al., 2012, Explanatory Supplement to the WISE All Sky Data Release
Damjanov I., Jayawardhana R., Scholz A., Ahmic M., Nguyen D. C., Brandeker A., van Kerkwijk M. H., 2007, ApJ, 670, 1337
Dawson P., Scholz A., Ray T. P., 2011, MNRAS, 418, 1231
de Bruijne J. H. J., Hoogerwerf R., Brown A. G. A., Aguilar L. A., de Zeeuw P. T., 1997, in Perryman M. A. C., Bernacca P. L., Battrick B., eds, ESA SP-402: Hipparcos – Venice '97 Improved Methods for Identifying Moving Groups. ESA, Noordwijk, p. 575
Dullemond C. P., Dominik C., 2004, A&A, 421, 1075
Dullemond C. P., Hollenbach D., Kamp I., D'Alessio P., 2007, Protostars and Planets V. Univ. Arizona Press, Tucson, p. 555
Ercolano B., Clarke C. J., Robitaille T. P., 2009, MNRAS, 394L, 141
Espaillat C., Calvet N., Luhman K. L., Muzerolle J., D'Alessio P., 2008, ApJ, 682L, 125

Espaillat C. et al., 2012, ApJ, 747, 103
Haisch K. E., Jr, Lada E. A., Lada C. J., 2001, ApJ, 553, L153
Hernandez J. et al., 2007, ApJ, 662, 1067
Jayawardhana R., Coffey J., Scholz A., Brandeker A., van Kerkwijk M. H., 2006, ApJ, 648, 1206
Lada C. J. et al., 2006, AJ, 131, 1574
Lawrence A. et al., 2007, MNRAS, 379, 1599
Lodieu N., Hambly N. C., Jameson R. F., 2006, MNRAS, 373, 95
Lodieu N., Hambly N. C., Jameson R. F., Hodgkin S. T., Carraro G., Kendall T. R., 2007, MNRAS, 374, 372
Lodieu N., Hambly N. C., Jameson R. F., Hodgkin S. T., 2008, MNRAS, 383, 1385
Lodieu N., Dobbie P. D., Hambly N. C., 2011, A&A, 527A, 24
Luhman K. L., 2004, ApJ, 602, 816
Luhman K. L., 2007, ApJS, 173, 104
Luhman K. L., Mamajek E. E., 2012, ApJ, 758, 31
Luhman K. L., Stauffer J. R., Muench A. A., Rieke G. H., Lada E. A., Bouvier J., Lada C. J., 2003, ApJ, 593, 1093
Luhman K. L. et al., 2005, ApJ, 631, L69
Martin E. L., Delfosse X., Guieu S., 2004, AJ, 127, 449
Mayne N. J., Naylor T., Littlefair S. P., Saunders E. S., Jeffries R. D., 2007, MNRAS, 375, 1220
Merin B. et al., 2010, ApJ, 718, 1200
Muzerolle J., Allen L., Megeath S. T., Hernandez J., Gutermuth R. A., 2010, ApJ, 708, 1107
Muzerolle J. et al., 2006, ApJ, 643, 1003
Natta A., Testi L., 2001, A&A, 376L, 22
Natta A., Testi L., Comern F., D'Antona F., Baffa C., Comoretto G., Gennari S., 2002, A&A, 393, 597
Oliveira J. M., Jeffries R. D., Kenyon M. J., Thompson S. A., Naylor T., 2002, A&A, 382L, 22
Pecaut M. J., Mamajek E. E., Bubar E. J., 2012, ApJ, 746, 154
Preibisch T., Zinnecker H., 1999, AJ, 117, 2381
Preibisch T., Brown A. G. A., Bridges T., Guenther E., Zinnecker H., 2002, AJ, 124, 404
Riaz B., Lodieu N., Goodwin S., Stamatellos D., Thompson M., 2012, MNRAS, 420, 2497
Scholz A., Jayawardhana R., Wood K., Meeus G., Stelzer B., Walker C., O'Sullivan M., 2007, ApJ, 660, 1517
Scholz A., Xu X., Jayawardhana R., Wood K., Eislöffel J., Quinn C., 2009, MNRAS, 398, 873
Sherry W. H., Walter F. M., Wolk S. J., 2004, AJ, 128, 2316
Skrutskie M. F. et al., 2006, AJ, 131, 1163
Slesnick C. L., Carpenter J. M., Hillenbrand L. A., 2006, AJ, 131, 3016
Slesnick C. L., Hillenbrand L. A., Carpenter J. M., 2008, ApJ, 688, 377
Wright E. L. et al., 2010, AJ, 140, 1868
Zapatero Osorio M. R., Bejar V. J. S., Pavlenko Ya., Rebolo R., Allende Prieto C., Martn E. L., Garca Lpez R. J., 2002, A&A, 384, 937

APPENDIX A: NEW OBJECTS FROM UKIDSS NINTH DATA RELEASE

This section outlines the method used to identify new brown dwarfs in UpSco using the UKIDSS Ninth Data Release. It is the same method as used by Dawson et al. (2011) to analyse the Eighth Data Release. For the sake of brevity, some of the details described by Dawson et al. (2011) are not repeated here.

UKIDSS is made up of several components including the Galactic Cluster Survey (GCS). Described in detail in Lawrence et al. (2007), the GCS is a survey of 10 large open star clusters and star-forming regions, including UpSco.

The instrument used to take the GCS images is the Wide Field Camera (WFCAM). Data collected by the WFCAM is subject to an automated process that detects and parameterizes objects and performs photometric and astrometric calibrations. The resulting reduced image frames and catalogues are then placed in the WFCAM Science Archive (WSA). The WSA can be interrogated using Structured Query Language (SQL).

As shown in Fig. A1, the new area in UpSco investigated here and surveyed for the Ninth Data Release covers 24 deg^2. The data for objects in the target area were obtained via an SQL query to the UKIDSS GCS data base. All queries were structured to include only point source objects in order to avoid contamination by extended sources (e.g. relatively nearby galaxies). As every object with photometric characteristics consistent with a brown dwarf had its proper motion assessed, in order to check whether it is likely a member of UpSco, each query submitted also correlated all objects found in the UKIRT GCS data bases with those found in 2MASS data bases. The 2MASS data are used as a first epoch for the purposes of proper motion calculation.

A1 Photometry

A query similar to that shown in Dawson et al. (2011) was submitted to the WSA. The query returned 1438 887 objects.

The objects were assessed on the basis of their position on a ($Z - J$, Z) colour–magnitude diagram as shown in Fig. A2. To refine the search, a new query was submitted to the WSA eliminating all objects to the left of a line in the ($Z - J$, Z) colour–magnitude diagram from ($Z - J$, Z) = (1.0, 14.0) through (1.4, 16.6) to (3.0, 21.55) (dashed line in Fig. A2). This query left 4398 objects. Reddening caused by extinction shifts objects to the right and down on colour–magnitude diagrams. To assess if reddening was contaminating the results, the 4398 objects had their location plotted as shown in the right-hand panel of Fig. A1. There is an obvious clustering of objects in a large area which coincides with the heavily extincted region around ρ Oph. Therefore, the analysis was confined to 706 638 objects in the Ninth Data Release that were outside that region (dashed lines in Fig. A1). This left only 200 of the 4398 objects selected in the initial ($Z - J$, Z) cut. These 200 objects were examined again in the ($Z - J$, Z) colour–magnitude diagram. 86 of the objects to the left of the line ($Z - J$, Z) = (1.1, 14.0) through (1.1, 14.3), (1.2, 14.9), (1.3, 15.2), (1.6, 17.0) to (3.0,21.0) were rejected for being too far from the isochrone on the blue side, leaving 114 photometric candidates.

A2 Proper motion

The 114 photometric candidates were then examined to find their proper motion. The resulting vector point diagram is shown in Fig. A3. The known proper motions of UpSco in right ascension and declination are about -11 mas yr^{-1} and -25 mas yr^{-1}, respectively (de Bruijne et al. 1997; Preibisch et al. 2002). Of the 114 candidates, 4 were too faint to be recorded in 2MASS leaving 110 candidates with proper motion data calculated. The remaining 110 candidates included 14 with proper motions greater than the range of Fig. A3.

All 96 candidates shown in Fig. A3 are predominantly centred around the (-11, -25) position. A 2σ selection circle as calculated in Dawson et al. (2011) is shown centred on that position. There is no significant clustering of objects around the (0,0) position indicating that the sample is not contaminated by more distant objects, e.g. AGB stars which have similar surface temperatures and colours to brown dwarfs, but much greater intrinsic luminosities. The 76 candidates within the 2σ selection circle were then classified as

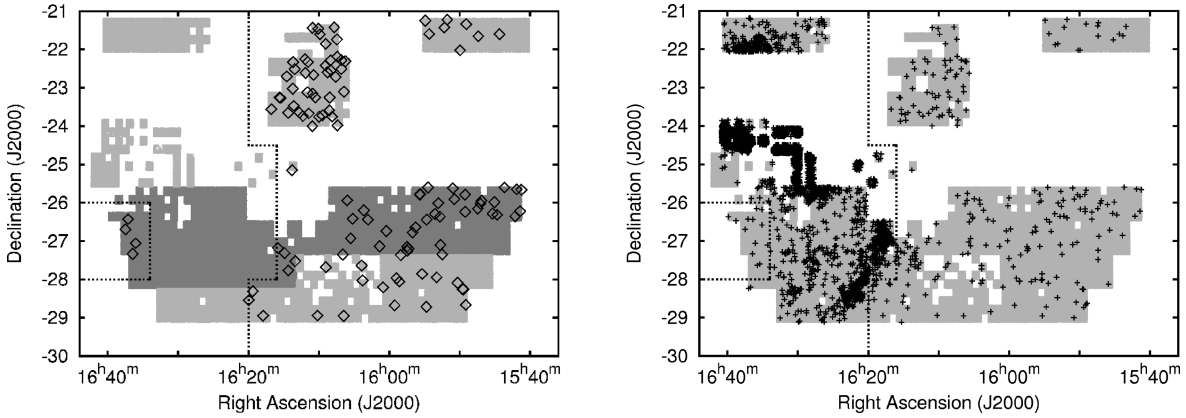

Figure A1. Coverage in Z, Y, J, H and K filters of 57 deg^2 in Upper Scorpius from the UKIDSS GCS. The left-hand panel shows the new 24 deg^2 of coverage from the Ninth Data Release in dark grey and earlier coverage in light grey. The open diamonds mark the position of the 116 brown dwarfs that comprise the sample analysed in this work. The right-hand panel shows the location of objects selected by the first cut in the ($Z - J$, Z) colour–magnitude diagram. 95 per cent of all the objects selected from the Ninth Data Release are clustered around the heavily extincted region surrounding ρ Oph. To obtain a minimally contaminated sample of brown dwarf candidates, the area inside the two sets of dashed lines was excluded from consideration.

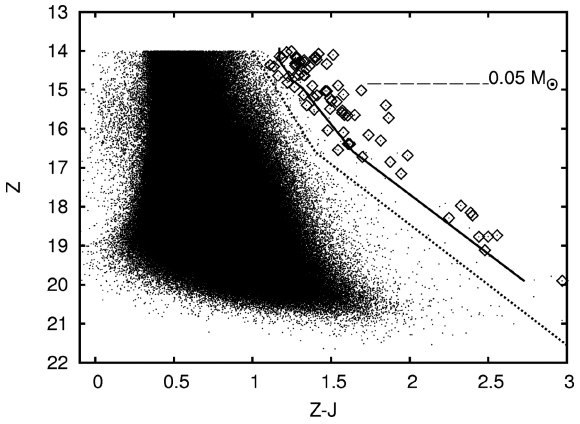

Figure A2. ($Z - J$, Z) colour–magnitude diagram showing the 76 brown dwarf candidates from the Ninth Data Release as open diamonds. All other objects are shown as small dots. The 5 Myr DUSTY model (Chabrier et al. 2000) isochrone is also shown with mass decreasing going down the isochrone from 0.09 $M_\odot$ at the top to 0.01 $M_\odot$ at the bottom. The 0.05 $M_\odot$ position on the isochrone is indicated. All objects to the left of the dashed line were rejected because of their colours.

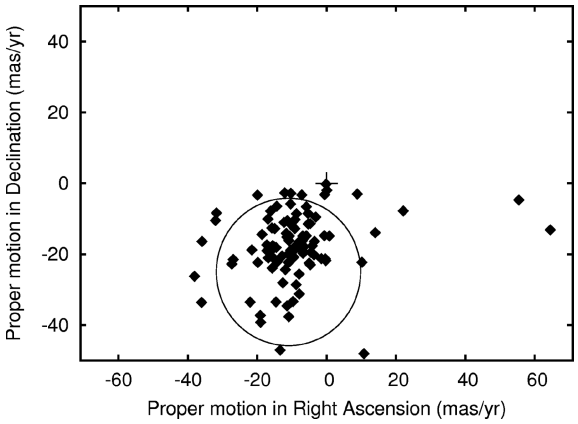

Figure A3. Vector point diagram for 96 candidate brown dwarfs in Upper Scorpius. There is an obvious and identifiable cluster around (−11, −25), while there is no significant clustering around the origin, indicating that there is very little contamination from background objects in the sample. Candidates lying outside the 2σ selection circle were classified as non-members, leaving 76 brown dwarf members of UpSco.

members of UpSco. These objects so selected have the photometric and proper motion characteristics of a 5 Myr old brown dwarf member of UpSco. 25 of the 76 were among the sample of 68 selected by Dawson et al. (2011), yielding 51 new objects from the Ninth Data Release to add to the sample. From these 51 brown dwarfs, 5 have been identified before. Lodieu et al. (2006) identify one of them, Martin et al. (2004) list another and Ardila et al. (2000) identify three. We note that the remaining 46 have not been previously identified in other surveys.

One potential caveat with respect to this sample is the fact that the Upper Scorpius population and the younger ρ Oph population are unlikely to be clearly separated in colour–magnitude or proper motion diagrams. By avoiding the areas with very high extinction (see Fig. A1), we exclude the bulk of the population of ρ Oph, but some scattered young substellar members of ρ Oph might still contaminate our sample. The low disc fraction in our sample, however, suggests that this cannot be a major factor.

APPENDIX B: SELECTED SPECTRAL ENERGY DISTRIBUTIONS

In this section, we show spectral energy distributions for 12 objects from our sample, 6 class II and 6 class III objects for comparison. The class III objects used have the closest magnitude in the J passband to the class II objects with which they are compared. Shown in the top panels of Fig. B1 are two of the typical examples that were deemed class II on the basis of their $W1$–$W2$ (3.4–4.6 μm) colour alone (as is the object featured in the left-hand panel in Fig. 6). The difference in slopes between the $W1$ and $W2$ points on the class II and class III spectral energy distributions are apparent, as are the higher $W3$ (12 μm) and $W4$ (22 μm) values of the class II objects. The two class II objects that stand out in Fig. 4 because of their large $J - K$ excess are shown in the middle panels of Fig. B1. Of all the 27 class II objects, the spectral energy distributions for these 2 show the greatest divergence from those of their corresponding class III

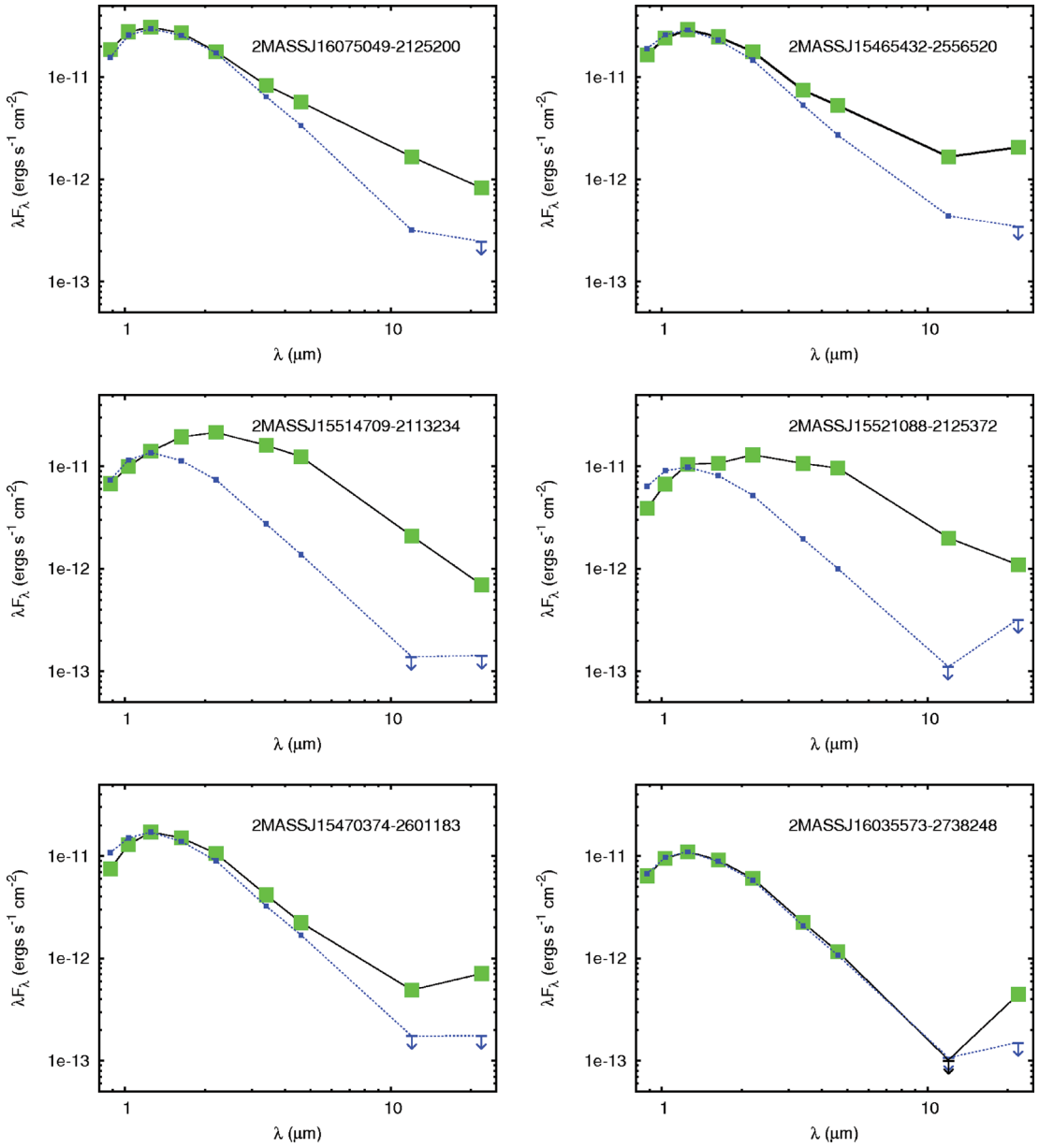

Figure B1. Spectral energy distributions for 6 of the 27 class II objects (solid lines with large squares) shown alongside 6 of the 89 class III objects (dotted lines with small squares). Detections with an S/N of < 5.0 are marked as upper limits. The class II objects in the top and middle panels are among the 22 distinguished using their $W1-W2$ (3.4–4.6 μm) colour alone. The middle panels show the two objects that also have the large $J-K$ excess, as well as having the brightest $W3$ signals, bright $W4$ signals and significant photometric variability (see Table 1). The class II objects in the bottom panels are two of the five with little or no $W1-W2$ excess that are included in the class II group on the basis of their bright $W3$ and/or $W4$ signals.

objects. The bottom panels in Fig. B1 show two of the five class II objects that could not be distinguished on the basis of their $W1-W2$ colour alone. (The right-hand panel in Fig. 6 features another of these objects.) The bottom-right panel is the most extreme example of all the five objects with little or no $W1-W2$ excess and deemed class II based on their bright $W3$ and/or $W4$ signals (the transition discs). It exhibits no $W1-W2$ excess and has a weak $W3$ signal. Apart from its strong $W4$ signal it resembles a class III object.

This paper has been typeset from a TEX/LATEX file prepared by the author.